ADVANCED FUNCTIONAL MATERIALS
www.afm-journal.de

Single-Crystal Organic Nanowire Electronics by Direct Printing from Molecular Solutions

*Kyung S. Park, Boram Cho, Jangmi Baek, Jae K. Hwang, Haiwon Lee, and Myung M. Sung**

A one-step process to generate single-crystal organic nanowire arrays using a direct printing method (liquid-bridge-mediated nanotransfer molding) that enables the simultaneous synthesis, alignment, and patterning of nanowires from molecular ink solutions is reported. Using this method, many single-crystal organic nanowires can easily be synthesized by self-assembly and crystallization of organic molecules within the nanoscale channels of molds, and these nanowires can then be directly transferred to specific positions on substrates to generate nanowire arrays by a direct printing process. The position of the nanowires on complex structures is easy to adjust, because the mold is movable on the substrates before the polar liquid layer, which acts as an adhesive lubricant, is dried. Repeated application of the direct printing process can be used to produce organic nanowire-integrated electronics with two- or three-dimensional complex structures on large-area flexible substrates. This efficient manufacturing method is used to fabricate high-performance organic nanowire field-effect transistors that are integrated into device arrays, inverters, and phototransistors on flexible plastic substrates.

1. Introduction

Organic nanowires have attracted great interest because of their structural flexibility, tunable optical and electrical properties, solution processability, and facile and large-scale synthesis.[1–4] From small-molecule single-crystals to crystalline polymers, they show intrinsic charge-transport properties and the highest performance due to single-crystal interfaces because of their nearly perfect translational symmetry and exceptionally high chemical purity.[5–9] Owing to the perfect order of molecules, the absence of grain boundaries, good contact interfaces, and a minimal number of charge traps, single-crystal organic nanowires have great potential for application in flexible, inexpensive, large-area applications such as flexible displays, radio frequency identification devices (RFIDs), smart cards, memory, solar cells, and sensors.[10–14] Even if their use has brought about significant advances in the area of organic electronics, there are still critical issues that must be overcome for large-scale application of these nanowires in practice. To use single-crystal organic nanowires in high-performance devices and large-scale integrated circuits, it is critical to synthesize and align individual nanowires precisely in the desired positions. Good alignment not only reduces and eliminates parasitic leakage paths, but also controls the azimuthal orientation of the nanowires in a single direction for optimal charge transport when fabricating devices.[8,15,16]

The general approaches for creating single-crystal organic nanowire devices are random casting of pre-grown nanowires onto substrates or alignment and/or placement of them into circuits by liquid-phase transfer and elastomeric stamping processes.[17–23] However, these processes are difficult for controlling individual nanowires with desired orientations and specific positions. Several fabrication methods for simultaneous synthesis and alignment of single-crystal organic nanowires directly on the device substrate surfaces have been developed, such as geometry-restricted evaporation induction, seed-induced growth, electrical field induction, magnetic field induction, liquid crystal assisted orientation, and nanoimprint lithography.[24–31] But, these methods still suffer from low quality of the nanowires and difficulty in well alignment of the individual nanowires. The only approach currently available for creating well aligned arrays of separate devices is manual selection and placement of individual organic nanowires; this process is prohibitive for producing a high density of device with reasonable throughput.[32–34]

Herein, we report the direct fabrication of single-crystal organic nanowire arrays from molecular solutions via a direct printing method, liquid-bridge-mediated nanotransfer molding (LB-nTM) method.[35] This simple method enables the simultaneous synthesis, alignment, and controlled positioning of single-crystal organic nanowires on substrates from molecular ink solutions. Organic molecules in ink solutions self-assemble and crystallize within the nanoscale channels of molds to form single-crystal nanowires, which are directly transferred to specific positions on the substrate to generate nanowire arrays. By using pre-patterned molds, organic nanowires arrays with tunable densities and intervals can be generated and aligned directly on the substrates. Furthermore, LB-nTM enables manipulation of the number of single-crystal organic nanowires

K. S. Park, B. Cho, J. Baek, J. K. Hwang, Prof. H. Lee, Prof. M. M. Sung
Department of Chemistry
Hanyang University
Seoul, 133-791, Korea
E-mail: smm@hanyang.ac.kr

DOI: 10.1002/adfm.201203540

incorporated in organic electronic devices. All successful organic nanowire device arrays reported to date have been fabricated by LB-nTM because this technique can produce two- or three-dimensional complex nanowire structures over large areas. In this study, we demonstrate how this method can be used to generate high-performance single-crystal organic nanowire transistors that can be integrated into organic nanowire inverter and phototransistor arrays on flexible substrates.

2. Results and Discussion

2.1. Single-Crystal Organic Nanowire Arrays

2.1.1. Fabrication of Single-Crystal Organic Nanowire Arrays

Figure 1a illustrates the procedure used to prepared single-crystal organic nanowire arrays by LB-nTM. Scanning electron microscope (SEM) images of representative structures formed in this manner are shown in Figure 1b–e. Molds are fabricated by casting polyurethane acrylate (PUA) on silicon wafers with nanoscale line patterns of resists (Figure 1b). Organic molecular ink solutions fill only the channels of the PUA molds due to selective inking based on discontinuous dewetting.[35,36] The inks inside the nanodiameter channels are solidified by drying at mild temperatures (<100 °C) (Figure 1c). In the ink solutions, the appropriate solvents with high boiling points (>200 °C) are used for reducing the evaporation rates. Thus, the organic molecules in the ink solutions slowly self-assemble and crystallize to form single-crystal organic nanowires within the nanoscale channels during solidification. The molds with single-crystal organic nanowires are brought into contact with substrate surfaces covered by a thin polar liquid layer, which forms a liquid bridge (a capillary bridge) between the substrate and the nanowires (Figure 1d). As the liquid evaporates, the attractive capillary force gradually increases, pulling the two surfaces into contact, and providing good conformal contact between them with no additional pressure to the mold. After drying, separation of the mold from the substrate yields single-crystal organic nanowire arrays (Figure 1e).

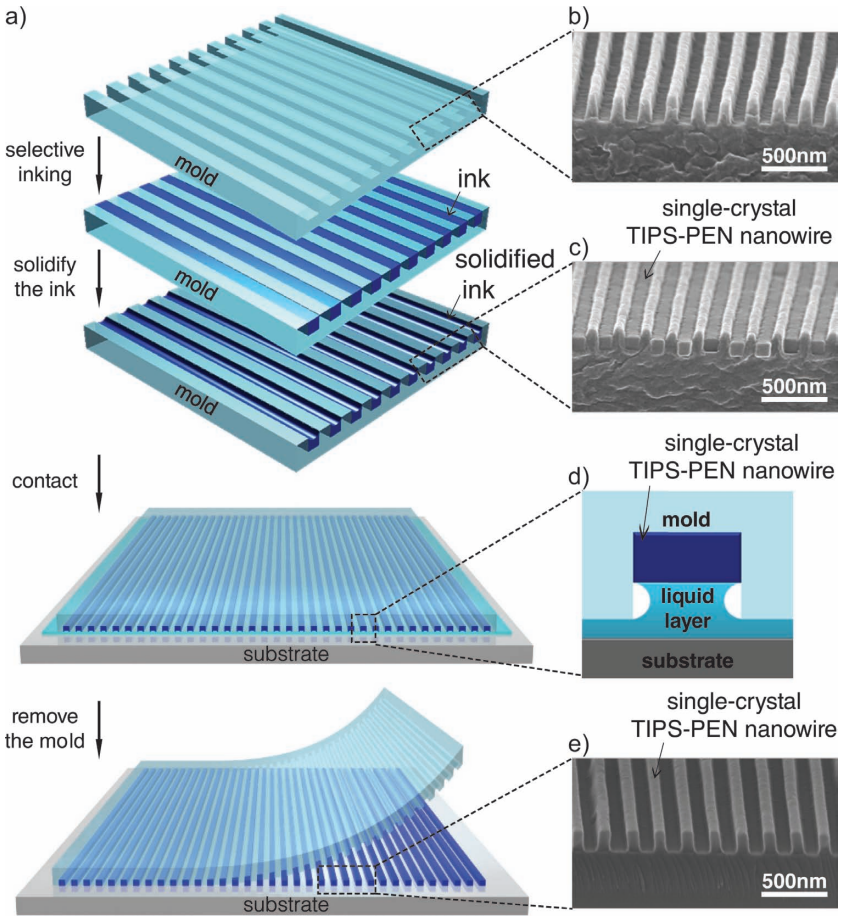

Figure 1. Fabrication of single-crystal organic nanowire arrays. a) Schematic illustration of the procedure used to fabricate single-crystal organic nanowire arrays on substrates using LB-nTM with a PUA mold. b) SEM image of the PUA mold with nanoscale patterns. c) SEM image of the mold filled with solidified TIPS-PEN inks (single-crystal TIPS-PEN nanowires). d) Schematic illustration of a liquid bridge formed by a polar liquid layer between the single-crystal TIPS-PEN nanowire and the substrate. e) SEM image of single-crystal TIPS-PEN nanowire arrays on the Si substrate.

Single-crystal organic nanowire arrays were made on Si substrates by LB-nTM using 6,13-bis(triisopropylsilylethynyl) pentacene (TIPS-PEN), fullerene (C_{60}), and poly(3-hexylthiophene) (P3HT) ink solutions. SEM images of single-crystal TIPS-PEN nanowire arrays fabricated using a mold (110 nm parallel lines and 90 nm spaces) clearly show that the nanowires with a width of 90 nm and a height of 138 nm are perfectly aligned to form 200 nm period arrays on the substrates (**Figure 2**a). Figure 2b shows SEM images of 200 nm period arrays of single-crystal C_{60} nanowires (110 nm width and 134 nm height) generated by LB-nTM using a mold with 90 nm parallel lines and 110 nm spaces. 200 nm period arrays of single-crystal P3HT nanowires (90 nm width and 132 nm height) were also fabricated using a mold (110 nm parallel lines and 90 nm spaces), as shown in Figure 2c. According to the cross-sectional SEM images, the organic nanowires showed various degree of roughness. The roughness of the nanowires highly depends on the nature of the molecules in the inks. Small molecules with large coplanar conjugate structures usually have smoother surfaces than polymers with long backbones and side chains. In this process, TIPS-PEN produced smoother nanowires than P3HT.

Furthermore, LB-nTM can be used to fabricate two- or three-dimensional complex nanowire arrays over a large area using a successive process, as shown in Figure S1, Supporting Information. A double layer structure was formed by consecutive printing of single-crystal TIPS-PEN nanowire arrays using LB-nTM (Figure 2d). The mold (550 nm parallel lines and 90 nm spaces) with the TIPS-PEN ink was placed in contact with the Si substrate, which had already been formed with one

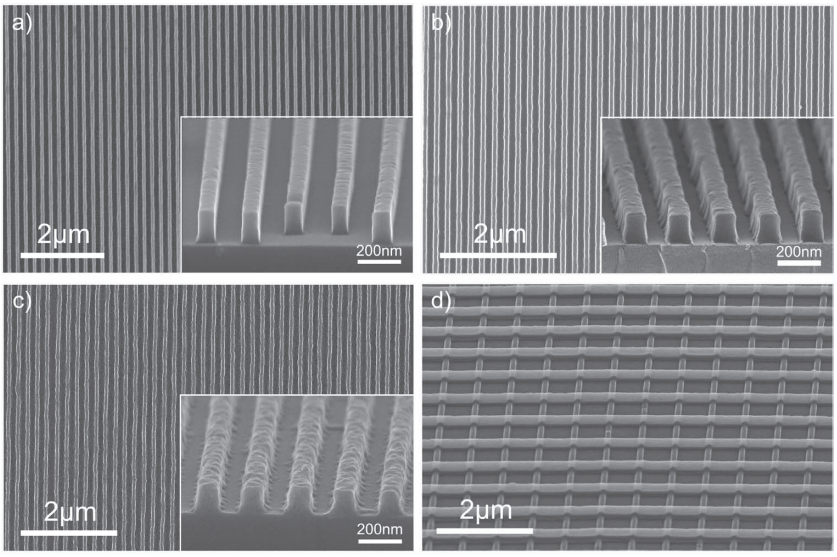

Figure 2. a) SEM image of TIPS-PEN nanowire arrays (white) fabricated by LB-nTM on a Si substrate (black). Inset: corresponding perspective magnified view of the nanowire arrays (nanowire width, W, 90 nm; spacing between nanowires, S, 110 nm; nanowire height, H, 138 nm). b) SEM image of C_{60} nanowire arrays. Inset: corresponding perspective magnified view of the nanowire arrays (W, 110 nm; S, 90 nm; H, 134 nm). c) SEM image of P3HT nanowire arrays. Inset: corresponding perspective magnified view of the nanowire arrays (W, 90 nm; S, 110 nm; H, 132 nm). d) SEM image (60° angled view) of a two-layer TIPS-PEN single-crystal nanowire array fabricated by repeated applications of LB-nTM on a Si substrate.

layer of the TIPS-PEN nanowire array. The mold was rotated 90° with respect to the direction of the first TIPS-PEN nanowires. The mold can be aligned easily on complex structures even after it is in contact with the substrate because before the polar liquid layer is dried, it acts as an adhesive lubricant, enabling movement of the mold over the substrate. LB-nTM is the most competitive fabrication method currently available for single-crystal organic nanowire arrays for organic electronic devices and integrated circuits.

2.1.2. Crystal Structures of Single-Crystal Organic Nanowires

The crystalline structures of the single-crystal organic nanowires were examined by selective-area electron diffraction (SAED) and X-ray diffraction (XRD). The TEM image and corresponding SAED patterns of the TIPS-PEN nanowire are shown in **Figure 3**a. The SAED patterns recorded from the three different regions along a TIPS-PEN nanowire clearly present very well-ordered diffraction spots, indicating that it is of single-crystalline nature. The detail structure of the nanowire was determined from the SAED patterns obtained from a tilting experiment.[37] For the analysis of the crystal structure, the lattices unit cell modeling and corresponding electron diffraction simulations, commercial software packages (Single Crystal 2.2.5. Crystal Maker Software Ltd.) were utilized.[38] The TIPS-PEN nanowire has a triclinic crystal structure with lattice dimensions of $a = 7.6$ Å, $b = 7.7$ Å, $c = 16.8$ Å, $\alpha = 89.2°$, $\beta = 92.7°$, $\gamma = 83.6°$.[39] The SAED data was further supported by the XRD pattern of the TIPS-PEN nanowires (Figure 3c). XRD was performed in reflection mode such that the scattering vector is perpendicular to the substrate (i.e., parallel to the nanowire axis). XRD pattern shows a well-defined set of (001) reflections, which indicates that the *c* axis of the TIPS-PEN crystals is oriented parallel to the surface normal with their *ab* planes on the substrates (Figure 3d).[40] These results indicate that single-crystal TIPS-PEN nanowires forms in the nanochannels of the molds along the [010] direction, which coincides with the π–π stacking direction of TIPS-PEN nanowires.

Microribbons were fabricated with TIPS-PEN by LB-nTM using a micro-patterned mold with 3 μm parallel lines and 2 μm spaces to compare with the nanowires made in the nanochannels. The SAED patterns

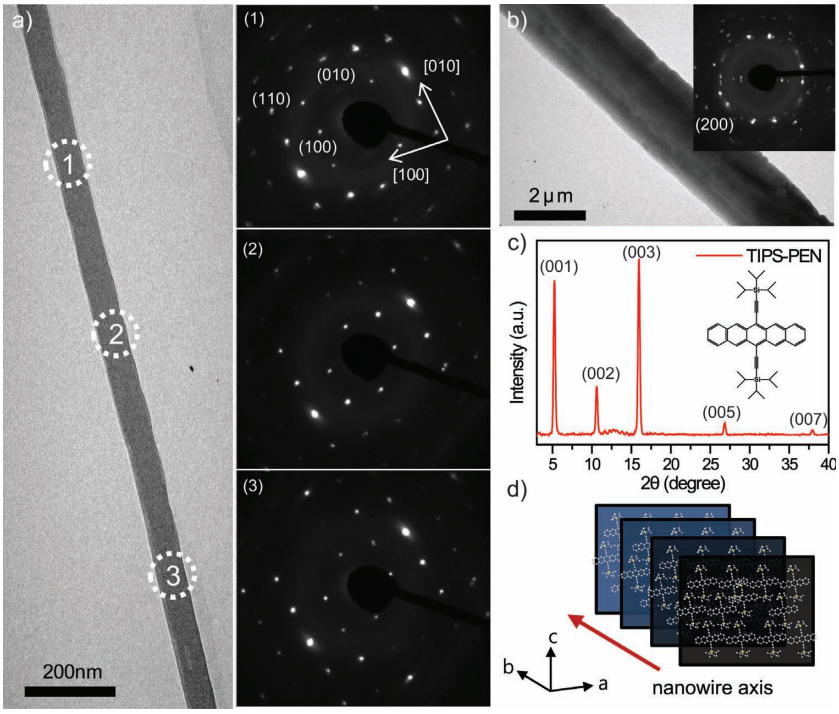

Figure 3. a) TEM image of the TIPS-PEN nanowire and the corresponding SAED patterns in different areas. The each area shows the single-crystalline nature. b) TEM image of microribbon of TIPS-PEN and the corresponding SAED pattern which indicates the semicrystalline nature. c) XRD patterns of TIPS-PEN nanowire arrays fabricated on the Si substrates by LB-nTM. d) Schematic representation of the crystal structure of single-crystal TIPS-PEN nanowire along the nanowire direction.

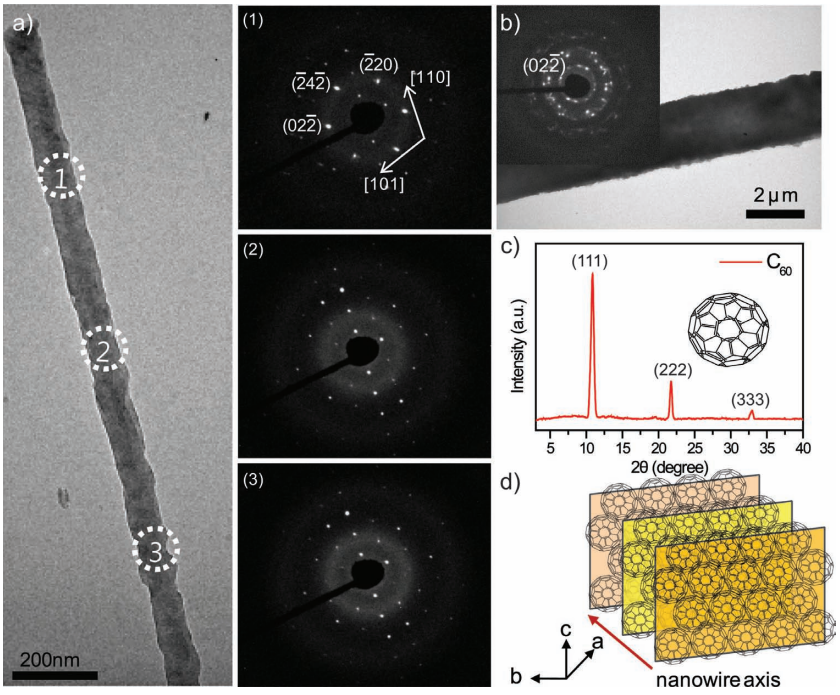

Figure 4. a) TEM image of the C_{60} nanowire and the corresponding SAED patterns in different areas. The each area shows the single-crystalline nature. b) TEM image of a C_{60} microribbon and the corresponding SAED pattern which indicates the semicrystalline nature. c) XRD patterns of C_{60} nanowire arrays fabricated on the Si substrate by LB-nTM. d) Schematic representation of the crystal structure of single-crystal C_{60} nanowire along the nanowire direction.

for the TIPS-PEN microribbon show many discrete diffraction spots in each Debye ring (Figure 3b), indicating that it has preferred-oriented semicrystalline ordering. This result could be attributed to crystallization of TIPS-PEN in the nanochannels of the molds during the LB-nTM process. It can therefore be concluded that the nanoconfinement effect provided by the nanochannels in the molds is crucial for the formation of the single-crystal TIPS-PEN nanowires in this method.[41]

Figure 4a shows the TEM image and corresponding SAED patterns obtained perpendicular to the length axis of the C_{60} single-crystal nanowire. The almost perfect single-crystalline nature of the C_{60} nanowire is confirmed by the SAED patterns, exhibiting exclusively reflections of the fcc structure oriented along the [111] zone axis, i.e., (101) and (110) spots. It is found that the $(02\bar{2})$ lattice spacing is 5.2 Å, which is similar to that obtained from fcc structured C_{60} nanorodes.[42] The SAED data was further supported by the XRD pattern of the C_{60} nanowires (Figure 4c). These results indicate that the C_{60} nanowire has a fcc crystal structure with cell dimensions of $a = b = c = 14.05$ Å, and forms in the nanochannels of the molds along the [110] direction (Figure 4d).[42,43] C_{60} microribbons (2 μm width) fabricated by LB-nTM have also preferred-oriented semicrystalline ordering, as shown in Figure 4b.

The P3HT nanowire also exhibit single-crystal diffraction spots in the SAED patterns and the polymer backbone of P3HT chains within the nanowire packed perpendicular to the nanowire long axis (**Figure 5**a). From the SAED patterns, it can be concluded that the P3HT nanowire has an orthorhombic crystal unit cell with lattice constants of $a = 16.6$ Å, $b = 7.8$ Å, and $c = 8.4$ Å, indicating a repetition unit of 8.4 Å along the polymer chain direction and a repetition unit of 7.8 Å along the π–π stacking direction.[44,45] The XRD patterns (Figure 5c) of the P3HT nanowires also confirm that the *a* axis of the P3HT crystals is oriented parallel to the surface normal with their *bc* planes on the substrates, as shown in Figure 5d. For comparison, P3HT microribbons were fabricated by LB-nTM using a micro-patterned mold with 3 μm parallel lines and 2 μm spaces. The SAED pattern in Figure 5b shows a diffused ring with d-spacing of 3.9 Å, which corresponds to the (020) plane of orthorhombic P3HT crystals.[46] This diffuse ring indicates that the microribbon is of polycrystalline or amorphous nature, which could be attributed to the nanoconfinement effect by the nanochannels in the molds during the LB-nTM process.

2.2. Single-Crystal Organic Nanowire Devices

2.2.1. Single-Crystal Organic Nanowire FET Arrays

We fabricated large-scale arrays of field-effect transistors (FETs) on 5 cm × 5 cm polyethersulfone (PES) substrates by LB-nTM using single-crystal TIPS-PEN nanowires as *p*-type active channels (**Figure 6**a). A 150-nm-thick indium-tin oxide (ITO) gate electrode and a 200-nm-thick SiO_2 dielectric layer were formed on a PES substrate by sputter deposition. Then, arrays of TIPS-PEN nanowires as active channel layers were fabricated on the substrate by LB-nTM. Finally, source and drain electrodes of 1.5-μm-thick Ag were defined to contact the TIPS-PEN nanowires on the substrate by LB-nTM. Figure 6b shows SEM images of the single-crystal TIPS-PEN nanowire FETs, with metal contacts functioning as source and drain electrodes and the ITO thin film as a back-gate. Note that the channel length was 5 μm. Figure 6c,d present typical drain current-gate voltage (I_D–V_G) transfer curves and drain current-drain voltage (I_D–V_D) output curves, respectively, for the FETs with 90 TIPS-PEN nanowires in the channel region. The TIPS-PEN nanowire FETs were well-modulated depending on the gate voltage and exhibited clear saturation behavior with a field-effect mobility of 1.52 $cm^2\ V^{-1}\ s^{-1}$, an on/off current ratio of ≈10^6, and a threshold voltage of −11 V. This performance is comparable to that of FETs containing one-dimensional TIPS-PEN single-crystals.[40,47] However, the measured mobility in our FETs is not representative of the intrinsic mobility of TIPS-PEN single-crystals because the output curves display a prominent contact resistance, which mainly comes from the energy barrier between Ag and TIPS-PEN and geometry charges in the interface due to the large height of the nanowires (138 nm). It should be noted that we made no effort to optimize device geometry or contact resistance. FETs with from 1 to 19 single-crystal TIPS-PEN

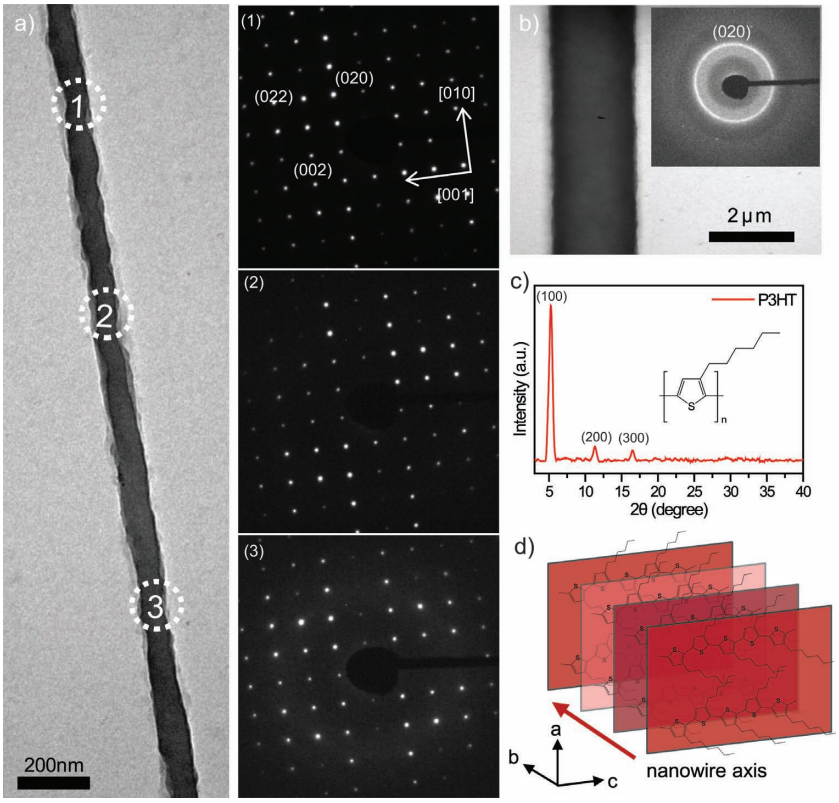

Figure 5. a) TEM image of the P3HT nanowire and the corresponding SAED patterns in different areas. The each area shows the single-crystalline nature. b) TEM image of P3HT microribbon and the corresponding SAED pattern which indicates the polycrystalline nature. c) XRD patterns of P3HT nanowire arrays fabricated on the Si substrate by LB-nTM. d) Schematic representation of the crystal structure of single-crystal P3HT nanowire along the nanowire direction.

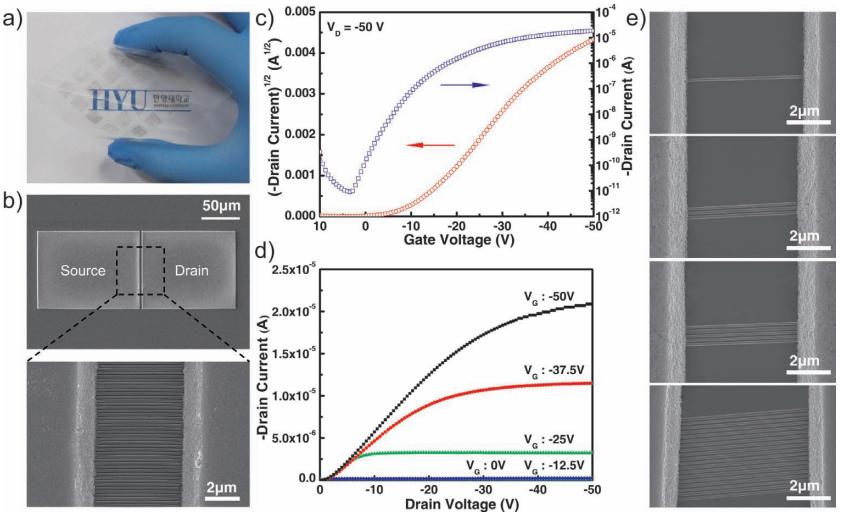

Figure 6. TIPS-PEN nanowire FETs. a) Photograph of an array of single-crystal TIPS-PEN nanowire FETs on a flexible substrate. b) SEM images of a typical nanowire FET where the Ag source-drain electrodes were defined by a subsequent LB-nTM. The bottom SEM image shows the well-aligned TIPS-PEN nanowire array channel between the Ag electrodes. c) Drain current–gate voltage (I_D–V_G) transfer curves (V_D = –50 V) of the FETs with 90 TIPS-PEN nanowires. The channel length is 5 μm. d) Drain current–drain voltage (I_D–V_D) output curves obtained from the same device. e) SEM images of FETs with 1 to 19 single-crystal TIPS-PEN nanowires.

nanowires were fabricated in a similar manner using LB-nTM (Figure 6e). The FET characters were modulated by the number of the nanowires in the channels, as shown in Figure S2, Supporting Information. Arrays of FETs with single-crystal C_{60} nanowires as *n*-type active channels were also fabricated on the PES substrates using LB-nTM (Figure S3, Supporting Information). The typical transfer and output characteristics of these FETs are shown in Figure S3b,c, respectively. The maximum I_D level was approximately 1 μA under a gate bias of 50 V. According to the transfer characteristics, a field-effect mobility of 0.12 $cm^2\ V^{-1}\ s^{-1}$ was achieved in the saturation regime of V_G = 50 V together with an on/off current ratio of ≈10^4 and a threshold voltage of 9 V. This performance is comparable to that of FETs containing C_{60} single-crystals.[48] Arrays of FETs with single-crystal P3HT nanowires as *p*-type active channels were also fabricated on the PES substrates using LB-nTM. The typical transfer and output characteristics of these FETs are shown in Figure S4, Supporting Information. The maximum I_D level was approximately 0.6 μA under a gate bias of –50 V. According to the transfer characteristics, a field-effect mobility of 0.08 $cm^2\ V^{-1}\ s^{-1}$ was achieved in the saturation regime of V_G = –50 V together with an on/off current ratio of ≈10^3 and a threshold voltage of –5.3 V. This performance is comparable to that of FETs containing needlelike P3HT single-crystals.[49] The single-crystal nanowire FETs were able to endure strenuous bending and were also transparent in the visible range, as shown in Figure 6a, and are therefore potentially useful for flexible and invisible electronics.

2.2.2. All Organic Nanowire Inverter Arrays

We integrated two FETs with single-crystal nanowires to generate large arrays of all organic nanowire inverters on 5 cm × 5 cm PES substrates using LB-nTM (**Figure 7**a). The schematic procedure to fabricate all organic nanowire inverter arrays is shown in Figure S5, Supporting Information. Note that each complementary inverter was fabricated using a single *p*-type TIPS-PEN and a single *n*-type C_{60} nanowire (Figure 7b). The fabrication of all organic nanowire inverter arrays was initiated by generation of single nanowire arrays of single-crystal TIPS-PEN on SiO_2/ITO-coated PES substrates as active *p*-channels using LB-nTM. Subsequently, a single C_{60} nanowire as an active *n*-channel was placed alongside the TIPS-PEN nanowire

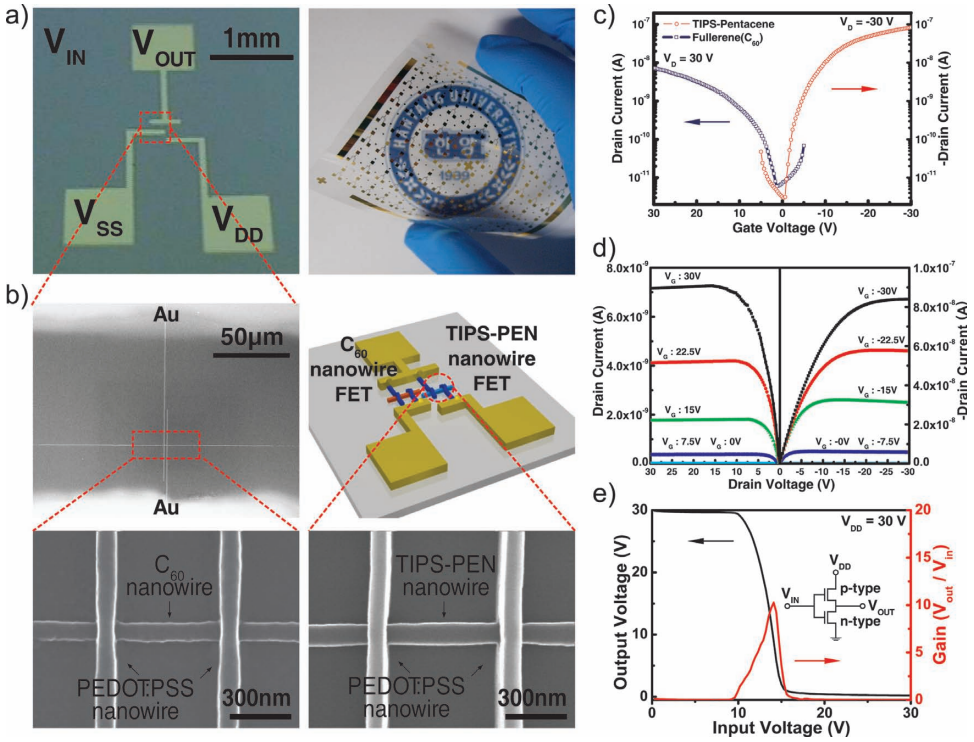

Figure 7. All organic nanowire inverter arrays. a) Photograph of large arrays of all organic nanowire inverters (right) and an optical image of a complementary inverter (left). b) Schematic of an inverter with a single TIPS-PEN and a single C_{60} nanowire contacting PEDOT:PSS nanowires as source and drain electrodes (top, right). Low magnification SEM image of a single C_{60} nanowire with a pair of PEDOT:PSS nanowires which was electrically connected by Au (top, left) and high magnification SEM images of a single C_{60} nanowire (bottom, left) and a single TIPS-PEN nanowire (bottom, right) with a pair of PEDOT:PSS nanowires, respectively. c,d) Drain current–gate voltage (I_D–V_G) transfer (c) and drain current–drain voltage (I_D–V_D) output (d) curves for the all organic nanowire FETs with a single *p*-type TIPS-PEN nanowire (right) and a single *n*-type C_{60} nanowire (left). e) Voltage-transfer characteristics of the complementary inverter and the corresponding voltage gain in the transition region where the gate threshold voltage is located.

using LB-nTM. Next, a pair of 90 nm PEDOT:PSS nanowires with 550 nm spacing was defined to contact the single TIPS-PEN and C_{60} nanowire on the substrates as the source and drain electrodes, respectively, by using LB-nTM.[50] Finally, two *p*-type and *n*-type FETs were electrically connected by evaporation of 200-nm-thick Au using a shadow mask (Figure S6, Supporting Information). Large arrays of the single-crystal organic nanowire inverters with PEDOT:PSS nanowires as source and drain electrodes and the ITO-coated PES substrate as a back gate, were thus obtained, as shown in Figure 7a.

Typical output and transfer curves for the all organic nanowire FETs show that these FETs have well-defined transistor characteristics with saturation effects (Figure 7c,d). The TIPS-PEN transistor had a field-effect mobility of 0.13 $cm^2\ V^{-1}\ s^{-1}$ in the saturation region at $V_{DS} = -30$ V, an on/off current ratio of $\approx 10^4$, and a threshold voltage of –2.3 V. The C_{60} FET had a field-effect mobility of 0.007 $cm^2\ V^{-1}\ s^{-1}$ in the saturation region at V_{DS} = 30 V, an on/off current ratio of $\approx 10^3$, and a threshold voltage of 1.5 V. The all organic nanowire transistors have a lower field-effect mobility than FETs with micron-sized metal electrodes because the 90 nm PEDOT-PSS nanowire electrode has lower conductance and a smaller contact area with the active nanowires than micron-sized metal electrodes. A schematic and SEM images of the inverter are provided in Figure 7b; a common gate (ITO) functioned as the input node (V_{in}) while the source of the driver was grounded and the source of the load transistor provided the supply voltage (V_{dd}). Figure 7e demonstrates typical voltage-transfer characteristics of the complementary inverters devised from single *p*-type TIPS-PEN and *n*-type C_{60} nanowires. Despite the fact that there was a large mismatch in charge carrier mobilities between the two semiconducting nanowires, a well-defined transfer curve was still observed with a relatively large gain of 10.

2.2.3. All Organic Nanowire Phototransistor Arrays

All organic nanowire phototransistor arrays were fabricated in the bottom gate, top contact FET configuration (**Figure 8**a). The schematic procedure to fabricate all organic nanowire phototransistor arrays is shown in Figure S7, Supporting Information. Note that we used a single P3HT single-crystal nanowire as a photosensitive semiconductor with PEDOT:PSS nanowire contacts functioning as source and drain electrodes and the ITO-coated PES substrate as a back gate (Figure 8a). A single P3HT nanowire was simultaneously synthesized and transferred to a specific position on the SiO_2/ITO-coated PES substrate by LB-nTM to generate photosensitive nanowire arrays. Then, a pair of 90 nm PEDOT:PSS nanowires with 550 nm spacing was defined to contact the P3HT nanowire on the substrate as the source and drain electrodes using LB-nTM. For electrical measurements, 200-nm-thick Au pads were deposited by evaporation using a shadow mask (Figure S8, Supporting

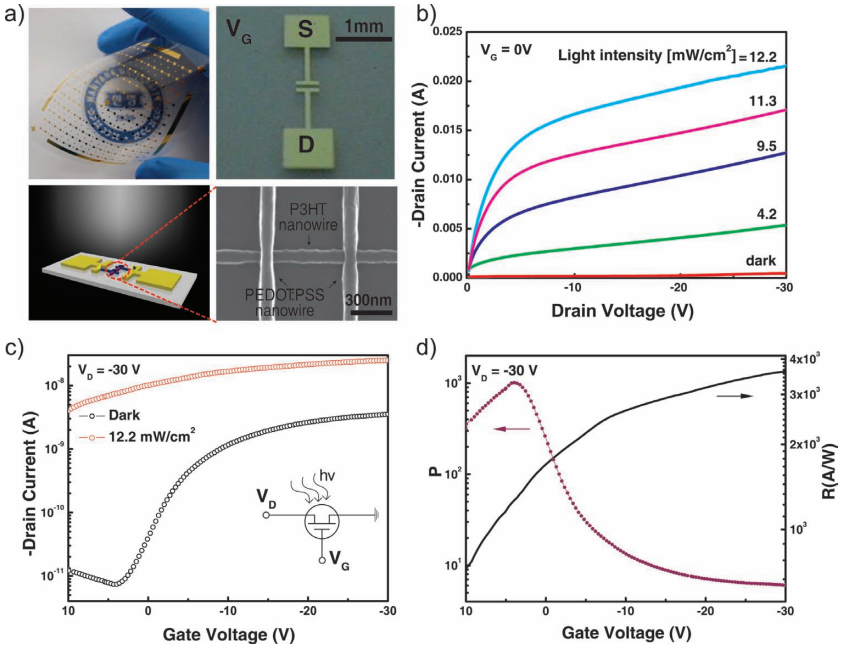

Figure 8. All organic nanowire phototransistor arrays. a) Photograph of large arrays of all organic nanowire phototransistors (top, left) and an optical image of a phototransistor (top, right). Schematic of a phototransistor with a single P3HT nanowire contacting PEDOT-PSS nanowires as source and drain electrodes (bottom, left) and an SEM image of P3HT and PEDOT-PSS nanowires comprising the phototransistor (bottom, right). b) Drain current–drain voltage (I_D–V_D) output curves obtained from the phototransistor at V_G = 0 V obtained by illumination of various intensities. c) Drain current–gate voltage (I_D–V_G) transfer curves (V_D = –30 V) of the P3HT nanowire phototransistor in dark and under a light intensity of 12.2 mW cm^{-2}. d) Responsivity (R) and photosensitivity (P) versus gate voltage (V_G) for the all organic nanowire phototransistor.

Information). The output characteristics of all organic nanowire phototransistors with a P3HT single-crystal nanowire are shown in Figure 8b, where I_{DS} is plotted as a function of the V_{DS} for different power densities of illumination (V_G = 0 V). The transistor was controlled by the incident light, and its output characteristics were very similar to those of organic FETs.[51,52] This suggests that the light could substitute for V_G as an independent variable to control the output of the transistor, indicating that a device with a single-crystal nanowire is capable of light detection and signal magnification, making it ideally suited for future low-cost, ultrahigh-density organic photoelectric integration. Typical transfer characteristics of the P3HT phototransistor measured in the dark (black circles) and under illumination (red circles, 12.2 mW cm^{-2}) are shown in Figure 8c. The P3HT transistor had a field-effect mobility of 0.007 cm^2 V^{-1} s^{-1} for both dark and light conditions, which value is comparable to that of FETs containing P3HT single nanofiber.[53] An obvious increase in I_{DS} was observed under illumination because of the contribution of the photocurrent. At V_G = 4 V, the transistor was charge-depleted in the dark. The maximum on/off ratio of the phototransistor was calculated to be 10^3 (V_G = 4 V). The performance of phototransistors is determined by their photosensitivity P (the ratio of the photocurrent to dark current) and responsivity R (the ratio of the photocurrent to the incident light intensity). The all organic nanowire phototransistors showed excellent photo response properties with a maximum P ($\approx 1 \times 10^3$) of and R (3.5×10^3 A W^{-1}) of under illumination with 12.2 mW cm^{-2} white light (Figure 8d).

3. Conclusions

In summary, we developed a direct printing method that enables the simultaneous synthesis, alignment, and controlled positioning of single-crystal organic nanowires from molecular ink solutions. We directly fabricated two- or three-dimensional integrated systems of the organic nanowires over a large area using repeated application of the direct printing process, which was facilitated by easy alignment of the mold on complex structures. This procedure can be used to generate various single-crystal organic nanowire arrays with controlled orientations and alignments on flexible substrates. Printed single-crystal organic nanowire arrays could potentially be used in all organic nanowire integrated electronics for transparent, flexible, inexpensive, and large-area applications.

4. Experimental Section

Materials: The TIPS-PEN ink solution was prepared by dissolving TIPS-PEN (2 wt%, ≥99%, Sigma Aldrich Inc.) in 1,2,3,4-tetrahydronaphthalene (tetralin, ≥97%, Sigma Aldrich Inc.) solvent. The C_{60} ink solution was prepared by dissolving C_{60} powder (1 wt%, 99.5%, Sigma Aldrich Inc.) in 1,3,5-trichlorobenzene (TCB, 99%, Sigma Aldrich Inc.). Regioregular P3HT (>98%, M_w = 40 kg mol^{-1}, Rieke Metals Inc.) was used to prepare the P3HT ink solution by dissolving P3HT (1.5 wt%) in 1, 3, 5-TCB. The Ag nanoparticle ink (DGP 40LT-15C) was purchased from Advanced Nano Products. The ink contained silver nanoparticles (20 wt%, particle diameter 40–50 nm) dispersed in methanol solvent. The PEDOT:PSS ink solution for highly conductive nanowire electrodes was prepared by addition of dimethylsulfoxide (DMSO) (7 wt%) to a PEDOT:PSS formulation (Clevios PH 510; H.C. Starck). Polyurethane acrylate (PUA) (MINS-ERM, Minuta Tech.) was used to prepare the UV-curable hard molds. Polydimethylsiloxane (PDMS) (Sylgard 184) was ordered from Dow Corning.

Preparation of Substrates: The Si substrates used in this research were cut from n-type (100) wafers with resistivity in the range of 1–5 Ω·cm. The Si substrates were initially treated by the chemical cleaning process to remove contaminants proposed by Ishizaka and Shiraki, which involves degreasing, HNO_3 boiling, NH_4OH boiling (alkali treatment), HCl boiling (acid treatment), rinsing in deionized water, and blow-drying with nitrogen.[54] A thin oxide layer was grown by placing the Si substrate in a piranha solution (4:1 mixture of H_2SO_4: H_2O_2) for 10–15 min. The substrate was rinsed several times in deionized water (resistivity = 18 MΩ·cm), then dried with a stream of nitrogen. The flexible substrates employed in this study were cut from Glastic polyethersulfone films (i-componenets Inc.). The polyethersulfone (PES) substrates were cleaned with methanol and de-ionized water, and finally blow-dried with nitrogen to remove contaminants.

Growth of Single-Crystal Organic Nanowires: Various single-crystal organic nanowire arrays were made on an oxidized Si(100) or PES substrate using the LB-nTM method with PUA molds. The masters used for fabrication of the molds were silicon wafers with dense or discrete

nanoscale line patterns, which were made by e-beam lithography. The molds were fabricated by casting PUA on them. After UV curing (≈10 min), the PUA molds were peeled away from the masters. To generate arrays of single-crystal organic nanowires, only recessed channels of the patterned PUA mold were filled with a TIPS-PEN, C_{60} or P3HT ink solution using discontinuous dewetting. By dragging a deposited ink solution over the patterned mold with a glass stick or a needle, the meniscus of the ink solution moved over the surface of the mold to fill the nano-diameter channels without leaving any residue on the raised surface. Discontinuous dewetting takes advantage of the interfacial free energy between the mold and the ink solution, and the ink solution must have a surface free energy (between ≈30 mJ m^{-2} and 70 mJ m^{-2}) appropriate for the PUA molds. The rate of dragging the solution, the aspect ratio of the features in the mold (depth/width ≥1/20), and the viscosity of the ink solution (<500 cP) also determine the success of the discontinuous dewetting process.

The ink in the nanoscale channels was next solidified by drying at mild temperatures below 100 °C for ≈30–60 min. During solidification, the organic molecules in the ink solution self-assembled and crystallized to form single-crystal organic nanowires within the nanoscale channels. The mold with the single-crystal organic nanowires was then brought into contact with a substrate surface covered by a thin ethanol layer. A substrate of area 1 cm × 1 cm was uniformly covered with a 100-μm-thick ethanol layer by using ethanol (10 μL). The ethanol layer on the substrate formed a liquid bridge (a capillary bridge) between the substrate and the mold that contained the single-crystal organic nanowires in channel patterns. The liquid bridge allowed good conformal contact between the nanowires and the substrate. As the ethanol evaporated, the attractive capillary force gradually increased, pulling the two surfaces into contact, and providing good conformal contact between them with no additional pressure on the mold. After drying, separation of the mold from the substrate yielded single-crystal organic nanowire arrays.

PEDOT:PSS nanowire electrodes were made on PES substrates using LB-nTM with the PUA molds. A PUA mold with nanoscale line patterns was filled with the PEDOT:PSS ink solution. The solidified PEDOT:PSS nanowires in the mold were transferred through the water layer to particular positions on the PES substrate with pre-patterned single-crystal organic nanowires using a liquid-bridge-mediated transfer process. Micrometer-scale Ag electrodes were made on the PES substrates using LB-nTM with a PDMS mold. The masters used for PDMS mold fabrication were silicon wafers with patterned resists on scales from 5 to 100 μm, which were made by photolithography. The molds were fabricated by casting PDMS on the masters. After curing at 70 °C for 50 min, the PDMS molds were peeled away from the masters. The PDMS molds were then filled with Ag solution. The solidified Ag electrodes in the molds were also transferred to specific positions of the PES substrate with pre-patterned single-crystal organic nanowires by liquid-bridge-mediated transfer.

Characterization: The samples were characterized using an optical microscope (ICS-305B, Sometech) and scanning electron microscope (SEM, Hitachi S4800) operated at 15 kV. The crystallinity of the organic nanowires was determined by a selective-area electron diffraction (EM 912 Omega) with a transmission electron microscope run at 120 kV and confirmed by X-ray diffraction (XRD, Bruker D8) using a Cu source run at 40 kV and 40 mA. All current–voltage (*I*–*V*) properties of the FETs and inverters were measured with a semiconductor parameter analyzer (HP 4155C, Agilent Technologies) in the dark and in air ambient (relative humidity ≈45%) at 20 °C. To characterize the phototransistor under illumination, a common incandescent lamp was employed as a light source. The power of the lamp was adjusted by a control knob, while the intensity was measured with a calibrated silicon photodiode. The field-effect mobility (μ) and threshold voltage (V_{th}) were calculated in the saturation regime (V_{DS} = −50, −30, 30, or 50 V) by plotting the square root of the drain current versus the gate voltage using $I_{DS} = (WC_i/2L)\mu(V_{GS}\text{-}V_{th})^2$, where C_i is the capacitance/unit area of the gate dielectric layer, and W and L are the channel width and length, respectively.

Supporting Information

Supporting Information is available from the Wiley Online Library or from the author.

Acknowledgements

K.S.P. and B.C. contributed equally to this work. This work was supported by the National Research Foundation (NRF) grant funded by the Korea government (MEST) (No. 2012-0008678), and the Global Frontier R&D Program on the Center for Multiscale Energy System (No. 2011-0031562), Nano•Material Technology Development Program (2012M3A7B4034985), and a Global Ph. D. Fellowship Program (No. 2011-0007507) funded by the National Research Foundation. We thank the Korea Basic Science Institute (KBSI) for allowing us to use their EF-TEM.

Received: November 30, 2012
Revised: February 13, 2013
Published online: April 9, 2013

[1] L. Zang, Y. Che, J. S. Moore, *Acc. Chem. Res.* **2008**, *41*, 1596–1608.
[2] Q. Tang, Y. Tong, Y. Zheng, Y. He, Y. Zhang, H. Dong, W. Hu, T. Hassenkam, T. Bjørnholm, *Small* **2011**, *7*, 189–193.
[3] Y. Tong, Q. Tang, H. T. Lemke, K. Moth-Poulsen, F. Westerlund, P. Hammershøj, K. Bechgaard, W. Hu, T. Bjørnholm, *Langmuir* **2010**, *26*, 1130–1136.
[4] K. Xiao, I. N. Ivanov, A. A. Puretzky, Z. Liu, D. B. Geohegan, *Adv. Mater.* **2006**, *18*, 2184–2188.
[5] A. L. Briseno, J. Aizenberg, Y.-J. Han, R. A. Penkala, H. Moon, A. J. Lovinger, C. Kloc, Z. Bao, *J. Am. Chem. Soc.* **2005**, *127*, 12164–12165.
[6] H. Moon, R. Zeis, E.-J. Borkent, C. Besnard, A. J. Lovinger, T. Siegrist, C. Kloc, Z. Bao, *J. Am. Chem. Soc.* **2004**, *126*, 15322–15323.
[7] V. Podzorov, E. Menard, Borissov, V. Kiryukhin, J. A. Rogers, M. E. Gershenson, *Phys. Rev. Lett.* **2004**, *93*, 086602.
[8] V. C. Sundar, J. Zaumseil, V. Podzorov, E. Menard, R. L. Willett, T. Someya, M. E. Gershenson, J. A. Rogers, *Science* **2004**, *303*, 1644–1646.
[9] R. Zeis, C. Besnard, T. Siegrist, C. Schlockermann, X. Chi, C. Kloc, *Chem. Mater.* **2006**, *18*, 244–248.
[10] H. E. A. Huitema, G. H. Gelinck, J. B. P. H. van der Putten, K. E. Kuijk, C. M. Hart, E. Cantatore, P. T. Herwig, A. J. J. M. van Breemen, D. M. de Leeuw, *Nature* **2001**, *414*, 599.
[11] R. Rotzoll, S. Mohapatra, V. Olariu, R. Wenz, M. Grigas, K. Dimmlerb, *Appl. Phys. Lett.* **2006**, *88*, 123502.
[12] R. J. Tseng, J. Huang, J. Ouyang, R. B. Kaner, Y. Yang, *Nano Lett.* **2005**, *5*, 1077–1080.
[13] S. Berson, R. De Bettignies, S. Bailly, S. Guillerez, *Adv. Funct. Mater.* **2007**, *17*, 1377–1384.
[14] S. C. Hernandez, D. Chaudhuri, W. Chen, N. V. Myung, A. Mulchandari, *Electroanalysis* **2007**, *19*, 2125–2130.
[15] S. De Vusser, S. Steudel, K. Myny, J. Genoe, P. Heremans, *Appl. Phys. Lett.* **2006**, *88*, 103501.
[16] K. C. Dickey, S. Subramanian, J. E. Anthony, L.-H. Han, S. Chen, Y.-L. Loo, *Appl. Phys. Lett.* **2007**, *90*, 244103.
[17] A. L. Briseno, S. C. B. Mannsfeld, X. Lu, Y. Xiong, S. A. Jenekhe, Z. Bao, Y. Xia, *Nano Lett.* **2007**, *7*, 668–675.
[18] A. L. Briseno, S. C. B. Mannsfeld, C. Reese, J. M. Hancock, Y. Xiong, S. A. Jenekhe, Z. Bao, Y. Xia, *Nano Lett.* **2007**, *7*, 2847–2853.
[19] Y. Zhou, W.-J. Liu, Y. Ma, H. Wang, L. Qi, Y. Cao, J. Wang, J. Pei, *J. Am. Chem. Soc.* **2007**, *129*, 12386–12387.

[20] L. Jiang, Y. Fu, H. Li, W. Hu, *J. Am. Chem. Soc.* **2008**, *130*, 3937–3941.
[21] J. H. Oh, H. W. Lee, S. Mannesfeld, R. M. Stoltenberg, E. Jung, Y. W. Jin, J. M. Kim, J.-B. Yoo, Z. Bao, *Proc. Natl. Acad. Sci. USA* **2009**, *106*, 6065–6070.
[22] C. Zhang, X. Zhang, X. Zhang, X. Ou, W. Zhang, J. Jie, J. C. Chang, C.-S. Lee, S.-T. Lee, *Adv. Mater.* **2009**, *21*, 4172–4175.
[23] S. Xiao, J. Tang, T. Beetz, X. Guo, N. Tremblay, T. Siegrist, Y. Zhu, M. Steigerwald, C. Nuckolls, *J. Am. Chem. Soc.* **2006**, *128*, 10700–10701.
[24] Y. Shoji, M. Yoshio, T. Yasuda, M. Funahashi, T. Kato, *J. Mater. Chem.* **2010**, *20*, 173–179
[25] I. O. Shklyarevskiy, P. Jonkheijm, P. C. M. Christianen, A. P. H. J. Schenning, A. D. Guerzo, J.-P. Desvergne, E. W. Meijer, J. C. Maan, *Langmuir* **2005**, *21*, 2108–2112.
[26] K. Xiao, I. N. Ivanov, A. A. Puretzky, Z. Liu, D. B. Geohegan, *Adv. Mater.* **2006**, *18*, 2184–2188.
[27] Y. Zhang, X. Wang, Y. Wu, J. Jie, X. Zhang, Y. Xing, H. Wu, B. Zou, X. Zhang, X. Zhang, *J. Mater. Chem.* **2012**, *22*, 14357–14362.
[28] Z. Wang, R. Bao, X. Zhang, X. Ou, C.-S. Lee, J. C. Chang, X. Zhang, *Angew. Chem. Int. Ed.* **2011**, *50*, 2811–2815.
[29] S. Samitsu, Y. Takanishi, J. Yamamoto, *Macromolecules* **2009**, *42*, 4366–4368
[30] Z. Zheng, K.-H. Yim, M. S. M. Saifullah, M. E. Welland, R. H. Friend, J.-S. Kim, W. T. S. Huck, *Nano Lett.* **2007**, *7*, 987–992.
[31] M. Cavallini, P. Stoliar, J.-F. Moulin, M. Surin, P. Leclère, R. Lazzaroni, D. W. Breiby, J. W. Andreasen, M. M. Nielsen, P. Sonar, A. C. Grimsdale, K. Müllen, F. Biscarini, *Nano Lett.* **2005**, *5*, 2422–2425.
[32] Q. Tang, H. Li, M. He, W. Hu, C. Liu, K. Chen, C. Wang, Y. Liu, D. Zhu, *Adv. Mater.* **2006**, *18*, 65–68.
[33] Q. Tang, H. Li, Y. Song, W. Xu, W. Hu, L. Jiang, Y. Liu, X. Wang, D. Zhu, *Adv. Mater.* **2006**, *18*, 3010–3014.
[34] Q. Tang, Y. Tong, W. Hu, Q. Wan, T. Bjørnholm, *Adv. Mater.* **2009**, *21*, 4234–4237.
[35] J. K. Hwang, S. Cho, J. M. Dang, E. B. Kwak, K. Song, J. Moon, M. M. Sung, *Nat. Nanotechnol.* **2010**, *5*, 742–748.
[36] R. J. Jackman, D. C. Duffy, E. Ostuni, N. D. Willmore, G. M. Whitesides, *Anal. Chem.* **1998**, *70*, 2280–2287.
[37] J. L. Lábár, *Ultramicroscopy* **2005**, *103*, 237–249.
[38] D. Golberg, M. Mitome, Ch. Müller, C. Tang, A. Leonhardt, Y. Bando, *Acta Mater.* **2006**, *54*, 2567–2576.
[39] J. E. Anthony, J. S. Brooks, D. L. Eaton, S. R. Parkin, *J. Am. Chem. Soc.* **2001**, *123*, 9482–9483.
[40] D. H. Kim, D. Y. Lee, H. S. Lee, W. H. Lee, Y. H. Kim, J. I. Han, K. Cho, *Adv. Mater.* **2007**, *19*, 678–682.
[41] Z. Hu, A. M. Jonas, *Soft Matter* **2010**, *6*, 21–28.
[42] H.-X. Ji, J.-S. Hu, L.-J. Wan, Q.-X. Tang, W.-P. Hu, *J. Mater. Chem.* **2008**, *18*, 328–332.
[43] S. Saito, A. Oshiyama, *Phys. Rev. Lett.* **1991**, *66*, 2637–2640.
[44] D. H. Kim, J. T. Han, Y. D. Park, Y. Jang, J. H. Cho, M. Hwang, K. Cho, *Adv. Mater.* **2006**, *18*, 719–723.
[45] X. Xiao, Z. Wang, Z. Hu, T. He, *J. Phys. Chem. B* **2010**, *114*, 7452–7460.
[46] S. Samitsu, T. Shimomura, S. Heike, T. Hashizume, K. Ito, *Macromolecules* **2008**, *41*, 8000–8010.
[47] D. H. Kim, D. Y. Lee, S. G. Lee, K. Cho, *Chem. Mater.* **2012**, *24*, 2752–2756.
[48] K. Ogawa, T. Kato, A. Ikegami, H. Tsuji, N. Aoki, Y. Ochiai, *Appl. Phys. Lett.* **2006**, *88*, 112109.
[49] X. Xiao, Z. Wang, Z. Hu, T. He, *J. Phys. Chem. B* **2010**, *114*, 7452–7460.
[50] C.-K. Cho, W.-J. Hwang, K. Eun, S.-H. Choa, S.-I. Na, H.-K. Kim, *Sol. Energy Mater. Sol. Cells* **2011**, *95*, 3269–3275.
[51] H. Jiang, X. Yang, Z. Cui, Y. Liu, H. Li, W. Hu, *Appl. Phys. Lett.* **2009**, *94*, 123308.
[52] Q. Tang, L. Li, Y. Song, Y. Liu, H. Li, W. Xu, Y. Liu, W. Hu, D. Zhu, *Adv. Mater.* **2007**, *19*, 2624–2628.
[53] J. A. Merlo, C. D. Frisbie, *J. Phys. Chem. B* **2004**, *108*, 19169–19179.
[54] A. Ishizaka, Y. Shiraki, *J. Electrochem. Soc.* **1986**, *133*, 666–671.